Brain Imaging and Behavior (2018) 12:1279-1289
https://doi.org/10.1007/s11682-017-9801-0

ORIGINAL RESEARCH

Network-level dysconnectivity in patients with nasopharyngeal carcinoma (NPC) early post-radiotherapy: longitudinal resting state fMRI study

Yingwei Qiu[1] · Zheng Guo[2] · Lujun Han[3] · Yadi Yang[3] · Jing Li[3] · Shiliang Liu[4] · Xiaofei Lv[3]

Published online: 21 November 2017

Abstract

In this study, we seek to longitudinally investigate the network-level functional connectivity (FC) alternations and its association with irradiation dose and cognition changes in the early stage post radiotherapy (RT) in nasopharyngeal carcinoma (NPC) patients. We performed independent component analysis (ICA) of resting state blood oxygen level-dependent functional magnetic resonance imaging (BOLD-fMRI) from 39 newly diagnosed NPC patients before receiving treatment (baseline), and 3 months post-RT. the default mode network (DMN), salience network (SN), and executive control network (ECN) were extracted with well-validated software (GIFT). Inter-network connectivity was assessed using the functional network connectivity (FNC) toolbox. The inter- and intra-network FC was compared between time points, and the z value of FC alternation was correlated with the RT dose value and cognitive changes. Compared with baseline, the FC of the left anterior cingulate cortex (ACC) within the DMN, and the right insular within the SN, significantly reduced 3 months post-RT, with greater effects at higher doses in the right insular. Bilateral ECN FC was also significantly lower 3 months post-RT compared to the baseline. Chemotherapy was not associated with inter- and intra- network FC change. We found intra- and inter-network FC disruption in NPC patients 3 months post-RT, with the right insular showing a dose-dependent effect. Thus, this network-level FC may serve as a potential biomarker of the RT-induced brain functional impairments, and provide valuable targets for further functional recovery treatment.

Keywords Radiotherapy · Nasopharyngeal carcinoma · Functional connectivity · Network · Resting-state functional magnetic resonance imaging

✉ Yingwei Qiu
qiuyw1201@gmail.com

✉ Xiaofei Lv
lvxf@sysucc.org.cn

[1] Department of Radiology, The Third Affiliated Hospital of Guangzhou Medical University, Guangzhou Medical University, Guangzhou 510150, People's Republic of China

[2] Department of Oncology, The First Affiliated Hospital of Ganzhou Medical University, Ganzhou, People's Republic of China

[3] Department of Medical Imaging Centre, State Key Laboratory of Oncology in South China, Collaborative Innovation Center for Cancer Medicine, Sun Yat-Sen University Cancer Center, Guangzhou, People's Republic of China

[4] Department of Radiation Oncology, State Key Laboratory of Oncology in South China, Collaborative Innovation Center for Cancer Medicine, Sun Yat-sen University Cancer Center, Guangzhou, People's Republic of China

Introduction

Nasopharyngeal carcinoma (NPC) is a malignant head and neck cancer, which has a relatively high incidence of 20–30 per 100,000 in endemic areas such as southern China and Southeast Asia (Wei and Sham 2005). Radiotherapy (RT) with or without adjuvant chemotherapy is the primary treatment modality for patients with NPC (Xu et al. 2017; Wei and Kwong 2010). RT is also well-acknowledged to contribute to neurological deterioration throughout the remaining lifetime of patients irradiated for NPC (Hsiao et al. 2010; Tang et al. 2012). However, the mechanism of this decline is poorly understood, and there is no effective prevention or long-term treatment. Traditionally, according to time of completion of RT, neurological side-effects induced by RT can be described in terms of acute (few days to few weeks), early delayed (1–6 months), and late delayed injury (>6 months) (Soussain et al. 2009). Research attention has

primarily focused on mechanisms of disability that appear at 6 months to 1 year after RT (Karunamuni et al. 2016; Seibert et al. 2017). However, recent studies showed that brain alterations and dysfunction develop much earlier (less than 6 months) following radiation exposure (Makale et al. 2017). Thus, the identification of an accurate and sensitive biomarker of brain damage and neurotoxicity in the early stage post RT is necessary to modify treatment strategies that may prevent or minimize brain damage.

Ideally, these biomarkers could be obtained during the course of standard treatment planning, and follow-up evaluation and would correlate with clinical outcome measures of cognitive function. However, such studies are quite scarce, and as mentioned above, most previous studies focused on the late delayed effects of RT. For example, following 15 high-grade glioma patients post-RT, Karunamuni et al. (Karunamuni et al. 2016) found cortical atrophy 1-year post-RT, with greater effects at higher doses, especially for the temporal and limbic cortex. Additionally, Seibert and colleagues (Seibert et al. 2017) reported that the hippocampus had radiation dose-dependent atrophy 1 year after treatment for patients who underwent fractionated, partial brain RT for primary brain tumors when compared to the baseline. Meanwhile Prust et al. (2015) revealed the volume of the whole brain and gray matter, but not the white matter and hippocampus, decreased during treatment, while the apparent diffusion coefficient increased within the subventricular zone 7 months after the initiation of chemoradiation treatment for glioblastoma. Recent studies also revealed that brain alterations and dysfunction developed much earlier following radiation exposure (Makale et al. 2017). By studying 22 patients with small cell lung cancer who underwent platinum-based chemotherapy and prophylactic cranial irradiation, researchers found that patients showed decreased volume in right subcortical regions, the bilateral insular cortex, superior temporal gyrus gray matter, and the right hippocampus and right para-hippocampal gyrus; this was accompanied by changes in the white matter microstructure of the entire corpus callosum 3 months post-treatment. Meanwhile, patients with non-small cell lung cancer showed no cognitive or brain structural differences after chemotherapy only, which suggests that chemotherapy, and especially prophylactic cranial irradiation, are associated with the development of cognitive and structural brain toxic effects (Simo et al. 2016). Using magnetic resonances spectroscopy (MRS) to investigate hippocampal metabolite, Pospisil and colleagues (Pospisil et al. 2017) found statistically significant decreases in h-tNAA in the bilateral hippocampus 4 months post whole brain RT in brain metastases patients when compared to baseline measurement. However, whether these imaging characteristics can serve as early biomarkers for the late toxicity of brain irradiation remains unclear, and correlation of these measures with neurocognitive function has yet to be established. Moreover, most of these findings focused on regional brain disruption (gray matter volume or metabolite) post-irradiation, and, as we know, anatomically separated regions of cortical grey matter are extensively interconnected. Thus, how the irradiation can induce the network-level functional connectivity (FC) disruption remains an open question. The application of novel neuroimaging techniques may provide additional insight into RT-related pathophysiology.

Resting-state FC magnetic resonance imaging (rs-fcMRI) is a method that can non-invasively assesses brain function (Zhang and Raichle 2010). rs-fcMRI measures the temporal correlation of spontaneous fluctuations of the blood oxygen level dependent (BOLD) signal between remote regions (Biswal et al. 1995). Correlated regions have been reproducibly classified into resting-state networks (RSNs) using both independent components analysis (Calhoun et al. 2001; Beckmann et al. 2005) and seed-based analysis (Damoiseaux et al. 2006; Shehzad et al. 2009). RSNs are of scientific interest because they recapitulate the topographies of task-related functional response (Beckmann et al. 2005; Smith et al. 2009). Importantly, rs-fcMRI eliminates performance confounds associated with task-based functional neuroimaging (Hyvarinen 1999; Ewers et al. 2011). Of the multiple RSNs that exist, 3 are particularly relevant to the study of loss of cognitive function in patients post irradiation because their irradiation related changes and associated cognitive alterations have been replicated in multiple studies (Greene-Schloesser and Robbins 2012; Zhang et al. 2015). The 3 RSNs are: the default mode network (DMN), the executive control network (ECN), and the salience network (SN) (Menon 2011). The DMN, including areas of the medial prefrontal cortex (MPFC), the posterior cingulate cortex (PCC), and the precuneus, is associated with internally oriented mentation and autobiographical memory (Gusnard et al. 2001; Fox et al. 2005); the ECN, mainly involving the dorsolateral prefrontal and the parietal regions, is engaged in higher-order cognitive processes and externally oriented attention (Bressler and Menon 2010); and the SN, comprising paralimbic structures—most prominently the anterior insular (AI) and medial frontal areas such as the anterior cingulate cortex (ACC) and pre-supplementary motor area (pre-SMA)—is involved in the switch between the DMN and task-related networks in cognitive control (Sridharan et al. 2008). The integrity of these 3 networks and their interactions appear fundamental to higher-level cognition, and are therefore relevant to our understanding of the brain injury related to RT (Greicius and Kimmel 2012).

The purpose of the present study was to longitudinally investigate network-level FC alternations, and their association with irradiation dose and cognition changes early post-RT in NPC patients.

Materials and methods

Patients

This prospective study was approved by the Institutional Review Board of the Sun Yat-sen University Cancer Center. Written informed consent was obtained from each subject before the study. From December 2014 to February 2017, 41 patients with newly diagnosed, histology-proven non-keratinizing undifferentiated NPC were enrolled, 2 patients were discarded due to excessive head movement during resting state fMRI scanning (more information can be found in the data preprocessing). Finally, 39 patients (25 M/14 F, aged 22–63 years old, 40.5 ± 8.4 years old) were included in this study. Each patient underwent a detailed pretreatment evaluation, including physical examination, nasopharyngeal fiberoptic endoscopy, chest radiography, MRI scan of the nasopharynx and brain, abdominal sonography, and whole body bone scan. The clinical stages of NPC were classified according to the American Joint Committee (AJCC) on Cancer Staging System (7th edition).

The inclusion criteria for all patients were as follows: no intracranial invasion, no distant metastases, no brain tumors, no alcoholism, no substance dependence, no neurological or psychiatric diseases, no prior substantial head trauma, no diabetes, no viral hepatitis, no positive human immunodeficiency virus status, no other major medical illness, not left-handed, and no contraindications for MRI scanning.

This prospective study was registered on the Chinese Clinical Trial Registry (http://www.chictr.org.cn/showproj.aspx?proj=11752). Registration Number: ChiCTR-OOB-15006982.

Treatment

All patients were treated using the intensity modulated RT (IMRT) technique, as previously described (Sultanem et al. 2000; Lin et al. 2014). Inverse planning was performed on the Corvus System (Peacock; Nomos, Deer Park, III) by using the simultaneous integrated boost technique. Target volumes were delineated slice-by-slice on treatment planning CT scans using an individualized delineation protocol that complies with International Commission on Radiation Units and Measurements reports 62 and 83. The prescribed radiation dose was as follows: a total dose of 68–70 Gy in 30–33 fractions at 2.12–2.27 Gy/fraction to the planning target volume (PTV) of the GTV-P, 60–70 Gy to the nodal gross tumor volume PTV (GTV-N), 60 Gy to the PTV of CTV-1 (high-risk regions), and 54–56 Gy to the PTV of CTV-2 (low-risk regions and neck nodal regions). All patients were treated with 1 fraction daily over 5 days per week. We then calculated the dose-volume statistics for temporal lobes, and outlined organs at risk for dose constraint evaluation. Dose-volume statistics for temporal lobes are listed in Table 1.

During the study period, institutional guidelines recommended RT alone for stage I, concurrent chemoradiotherapy for stage II, and concurrent chemoradiotherapy with/without neoadjuvant/adjuvant chemotherapy for stage III to IVA-B. Concurrent chemotherapy was cisplatin weekly (40 mg/m^2) or on weeks 1, 4, and 7 of RT (80–100 mg/m^2). Neoadjuvant chemotherapy consisted of cisplatin (80 mg/m^2) with 5-fluorouracil (750–1000 mg/m^2) (PF), or cisplatin (75 mg/m^2) with docetaxel (75 mg/m^2) (TP), or cisplatin (60 mg/m^2) with 5-fluorouracil (600 mg/m^2) and docetaxel (60 mg/m^2) (TPF) every 3 weeks for 2 or more cycles. In total, 3 patients (7.7%) belonged to AJCC stage II, and 36 (92.3%) patients with stage III-IV received neoadjuvant chemotherapy; all 39 patients (100%) received concurrent chemotherapy.

MRI acquisition

All MRI scans were performed on a GE Discovery MR750 3.0 Tesla scanner (GE Medical Systems, Milwaukee, WI) equipped at the Department of Medical Imaging, Sun Yat-sen University Cancer Center. Tight but comfortable foam padding was used to minimize head motion, and ear plugs were used to reduce scanner noise. For each patient, clinically routine MRI, including thick-slice T2- and T1-weighted images as well as T2 fluid-attenuated inversion recovery images were obtained to ensure that there were no visible brain lesions. Then, an rs-fMRI scan with an echo-planar imaging sequence and a high-resolution structural MRI scan with T1-weighted 3-dimensional brain volume imaging (3D-BRAVO) sequence were

Table 1 Demographic and clinical characteristics of NPC patients

Demographic information	Baseline
Age (Years)	40.5 (8.4)
Gender (M/F)	25/14
Education	12.0 (3.3)
Hypertension (−/+)	37/2
Diabetes (−/+)	39/0
Tumor stage (II/III/IV)	3/17/19
Temporal.R dose (maximum)	69.3 (6.9)
Temporal.R dose (minimum)	2.1 (1.2)
Temporal.R dose (mean)	20.4 (6.8)
Temporal.L dose (maximum)	68.4 (6.8)
Temporal.L dose (minimum)	2.2 (1.2)
Temporal.L dose (mean)	19.7 (6.2)

sequentially conducted. The imaging parameters were as follows: (1) rs-fMRI: repetition time (TR) = 2000 ms, echo time (TE) = 30 ms, flip angle = 90°, acquisition matrix = 64 × 64, field of view = 240 × 240 mm^2, 39 axial slices, slice thickness = 3 mm, inter-slice gap = 0.8 mm, voxel size = 3.75 × 3.75 × 3.8 mm^3, 240 time points (8 min); and (2) 3D-BRAVO: TR = 8.16 ms, TE = 3.18 ms, inversion time = 800 ms, flip angle = 8°, acquisition matrix = 256 × 256, field of view = 256 × 256 mm^2, 176 sagittal slices, no inter-slice gap, and voxel size = 1 × 1 × 1 mm^3. During rs-fMRI scanning, patients were instructed to close their eyes and keep still as much as possible, and to not think of anything systematically or fall asleep.

Neurocognitive tests

The Montreal Cognitive Assessment (MoCA, Beijing Version) was used to assess general cognitive function of NPC patients before treatment and 3 months post-treatment. The MoCA assesses different cognitive domains: attention and concentration, executive functions, memory, language, visuoconstructional skills, conceptual thinking, calculations, and orientation. The time to administer the MoCA for each patient is approximately 10 min, and the score range is from 0 to 30. All patients completed the MoCA after an appropriate demonstration and explanation, on the same day as MRI scanning.

Follow-up procedure

To assess the early RT-related network-level dysfunction (acute injury and early delayed injury), NPC patients were evaluated on the following time points: prior to the initiation of their treatment (baseline), immediately after completion of the neoadjuvant chemotherapy treatment (for patients who were treated with neoadjuvant chemotherapy), and 3 months following the completion of the concurrent RT. At each time-point, brain structural and functional MRI, and nasopharynx and/or neck MRI, as well as neurocognitive tests were performed. Figure 1 illustrates the procedures for follow-up of patients with NPC in this study.

Data pre-processing and isolation of independent components

Pre-processing of imaging data was performed using SPM8 (Wellcome Trust Centre for Neuroimaging, University of College London, UK) and following our previous work (Qiu et al. 2011, 2016, 2017a, b; Lv et al. 2013a, b, 2016), which included removal of the first 10 time-points to allow magnetization to reach steady state, slice-timing correction, and motion-correction. Dataset with motion exceeding 2 mm in any of the 3 cardinal directions (i.e., x, y, z) were removed from analysis. Functional images were then normalized to the MNI-152 template using non-linear transformation in SPM8, and smoothed using a 6 mm full width high maximum (FWHM) Gaussian kernel. Signals from known nuisance variable (e.g., cerebral spinal fluid, motion parameters) were not explicitly removed by regression. This information was used in the group independent component analysis (group ICA) to identify the independent components.

Group spatial ICA was conducted for both time points of all 39 subjects using the infomax algorithm within the GIFT software (http://icatb.sourceforge.net/) and following our previous work (Ma et al. 2015), which incorporated temporal concatenation plus back-reconstruction (which produces subject-specific images) (Calhoun et al. 2001). This enabled a comparison of both the time courses and the images for 1 group or multiple groups (Calhoun et al. 2001). A detailed

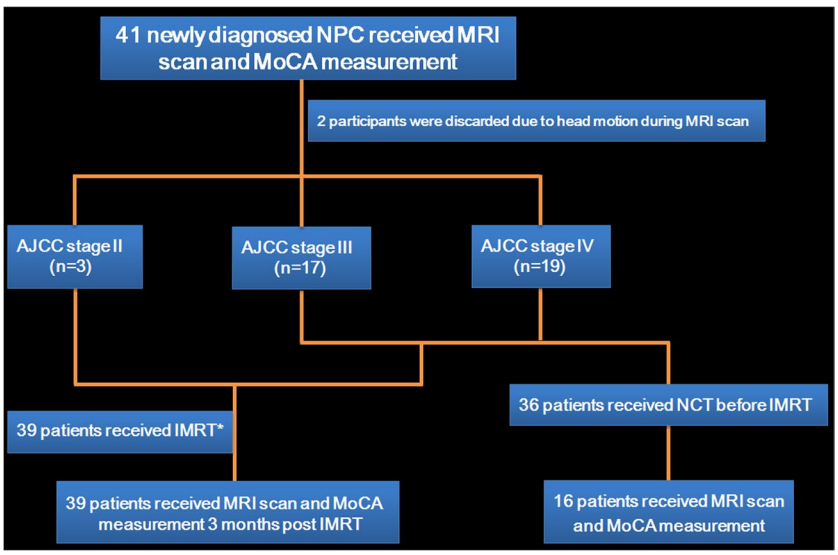

Fig. 1 Flow diagram of patient enrolment. * Patients underwent concurrent IMRT and chemotherapy. Abbreviation: NPC, nasopharyngeal carcinoma; MoCA, Montreal cognitive assessment, IMRT, intensity modulated radiotherapy; NCT, neoadjuvant chemotherapy

review of group ICA fMRI analyses can be found in the report by Calhoun et al. (Calhoun et al. 2009). In this study, images were reduced to 40 dimensions using principal component analysis, and the optimal number of components was found to be 34 using the minimum description length criteria modified to account for spatial correlation (Li et al. 2007). We applied the ICASSO algorithm implemented in GIFT to increase the robustness of our independent components to initial algorithm conditions by repeating the ICA estimation 100 times. Single subjects' spatial maps and corresponding time courses were then computed and converted to z-scores for display and use in further statistical analyses. Each voxel in the brain has a z-score representing the strength of its contribution to the component's time course. We selected DMN, ECN, and SN components using an automated and objective method. In detail, we chose representing subsystems of SN, DMN and ECN from the network template (Shirer et al. 2012) (http://findlab.stanford.edu/functional_ROIs.html), and performed multiple spatial regression analyses of our 34 independent components' spatial maps on these templates. We selected components with the highest correlation coefficient with the templates. In addition, all selected components were also visually inspected by 2 researchers to ensure the selected DMN, ECN, and SN corresponded to cerebral components with the largest spatial correlations with the network templates (van de Ven et al. 2004). Using this data-driven analysis approach allowed us to estimate FC without making any prior assumptions on how intrinsic activity is implemented.

Network-level FC evaluation of intra-network

Intra-network FC differences between pre- and post-RT were examined using a SPM8 paired t-test on the spatial distribution of the components (pDMN, aDMN, rECN, lECN and SN). Statistical images (t maps) were corrected for multiple-comparison using a AlphaSim correction. By using this program, a corrected significance level of $p < 0.05$ was obtained by clusters with a minimum volume of 2025 mm^3 at an uncorrected individual voxel height threshold of $p < 0.01$.

Network-level FC evaluation of inter-network

For this functional network connectivity analysis, inter-network connectivity reflective of between-network communication was assessed for differences between the pre- and post-RT using the Functional Network Connectivity (FNC, FncVer2.3) toolbox. FNC was calculated following the procedure described by Jafri et al. (2008). The number of component-pairs (comp-pair) was obtained from a computation of the number of components ($n = 5$). In each population group, we identified high-correlation component-pairs defined with a liberal threshold of Pearson's rho coefficient > 0.3. Furthermore, only the overlap of high correlation component-pairs ($n = 7$) between populations were statistically tested. Correction for multiple comparisons was implemented using false discovery rate (FDR) approach following the procedure introduced by Storey (2002).

Results

Demographic and cognitive measures

The demographic information for the NPC patients at baseline is shown in Table 1. The NPC patients had lower MoCA scores 3 months post-RT when compared with the baseline (Fig. 2).

Spatial distribution of DMN, ECN, and SN

Spatial distributions of DMN, ECN, and SN for NPC patients are shown in Fig. 3. The spatial distribution of the 3 particular networks was the same as those found by previous studies (Raichle et al. 2001; Qiu et al. 2017b).

Irradiation-related intra-network (DMN and SN) FC alternations in NPC patients

Individuals groups comparisons demonstrated significant differences between pre- and 3 months post-RT ($P < 0.05$, AlphaSim-corrected). After RT, NPC patients had weaker intra-network connectivity in the left ACC for the DMN, and the right insular for the SN (Fig. 4 and Table 2).

Irradiation-related inter-network (Bilateral ECN) FC alternations in NPC patients

Functional network connectivity for NPC patients before and 3 months post-RT shared similar connectivity diagrams, in

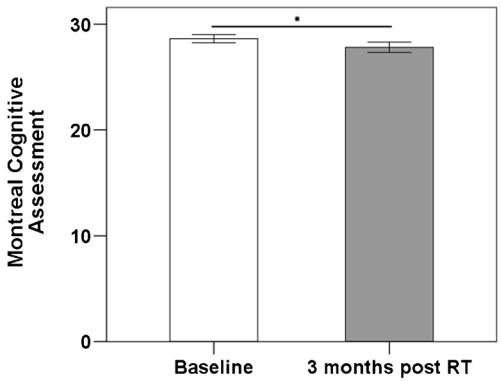

Fig. 2 NPC patients had significantly reduced MoCA 3 months post-RT. * $p < 0.05$

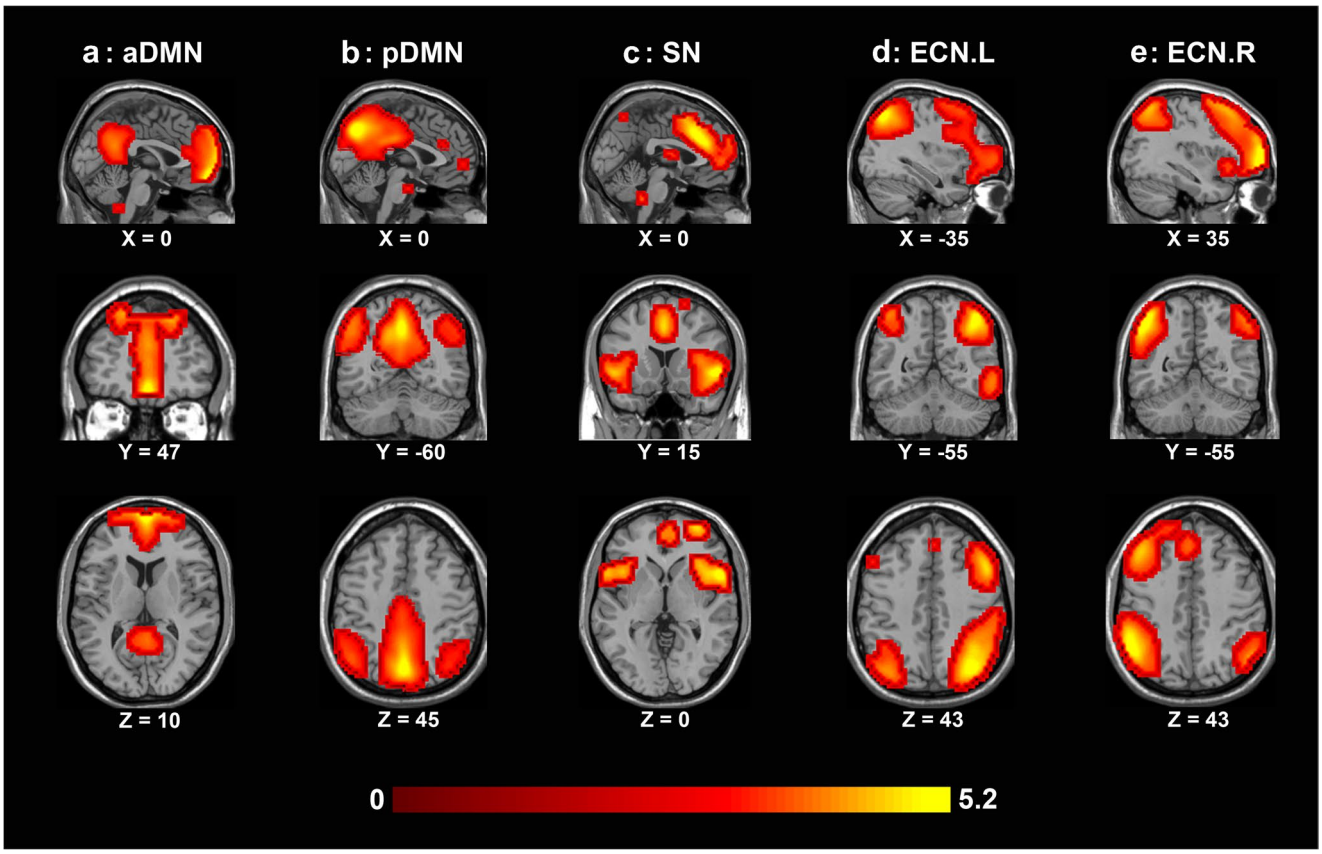

Fig. 3 Group level aDMN, pDMN, SN, left ECN and right ECN connectivity in NPC patients with both time points. Abbreviation: NPC, nasopharyngeal carcinoma; aDMN, anterior default mode network; pDMN, posterior default mode network; SN, salience network; ECN, executive control network

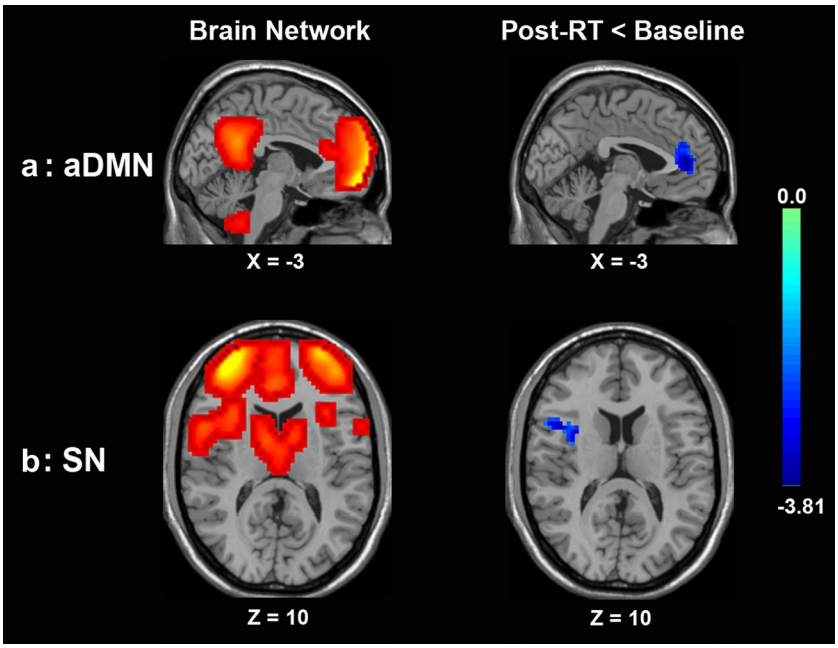

Fig. 4 Group comparison maps of intra-network differences (SN and DMN) in NPC patients between time points ($P < 0.05$, AlphaSim-corrected). After RT, NPC patients had weaker intra-network connectivity in the left ACC for the DMN (**a**), and the right insular for the SN (**b**) compared to the baseline. The coordinates of significantly different regions are shown in Table 2. Abbreviation: NPC, nasopharyngeal carcinoma; ACC, anterior cingulate cortex; DMN, default mode network; SN, salience network

Table 2 Intra-network functional connectivity (FC) alternation 3 months post-RT

Network	Region	Coordinate (MNI)	Brodmann area (BA)	Cluster size (mm^3)	Peak T-score
aDMN	ACC	−3,42,9	24,32	4131	−3.3814
SN	Insular	34,19,10	13,44	2133	−3.8117

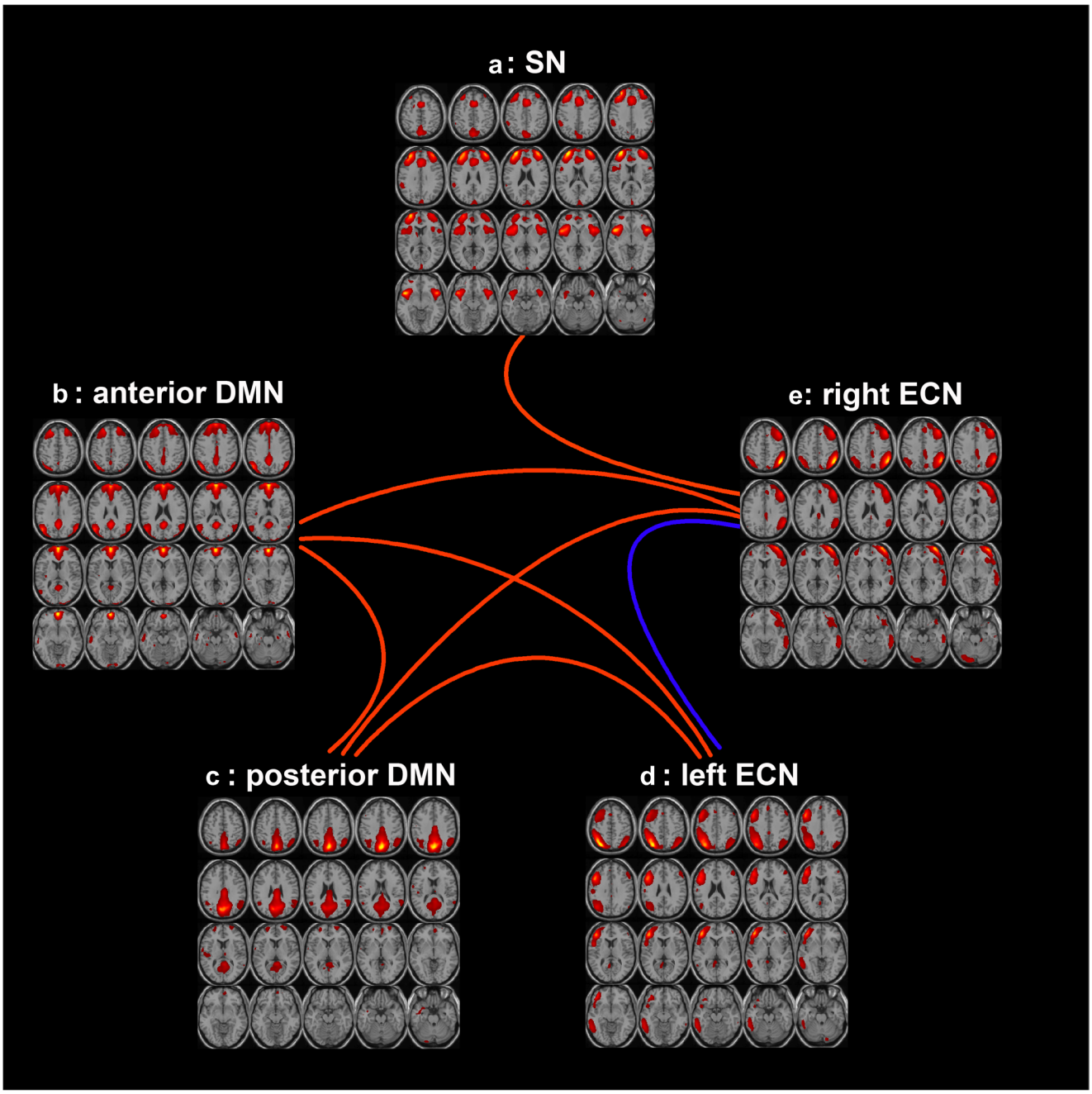

Fig. 5 Group comparison maps of inter-network differences in NPC patients between time points. Functional network connectivity for NPC patients before and 3 months post RT shared similar connectivity diagrams, in which significantly correlated components are represented by lines (A-E, B-C, B-D, B-E, C-E, C-D, and D-E). The blue line represents connectivity in which 3 months post treatment had lower mean correlation than baseline (D-E). Abbreviation: NPC, nasopharyngeal carcinoma; DMN, anterior default mode network; SN, salience network; ECN, executive control network

which significantly correlated components are represented by lines (Fig. 5). Blue line represents connectivity in which 3 months post treatment had lower mean correlation than baseline (Fig. 5).

No chemotherapy-related network-level FC alternations in NPC patients

To elucidate the chemotherapy effects on the network-level FC alternations, we also compared the intra- and inter- network FC in a sub-cohort sample (16 subjects) who had MRI examination and MoCA evaluation after completion of neoadjuvant chemotherapy but before the initial of RT. However, we did not find any intra- or inter- network FC changes related to chemotherapy.

Irradiation dose on the right temporal correlated with the right insular FC alternations

Changes in the right insular FC 3 months post-RT were negatively correlated with the maximum dose of irradiation of the right temporal lobe ($r = -0.402$, $p = 0.01$; Fig. 6).

Discussion

Quantification of network-level FC of normal appearing brain tissue after RT may help us understand the physiologic processes that underlie radiation-induced neurocognitive decline. Our results showed that both the intra-network (DMN and SN) and the inter-network (bilateral ECN) FC significantly reduced 3 months post-RT in NPC patients. Furthermore, the FC changes of the right insular within the SN had a dose-dependent effect (Fig. 6). Together, these findings suggested that the altered FC pattern might serve as a potential biomarker of radiation-induced brain dysfunctions in NPC patients.

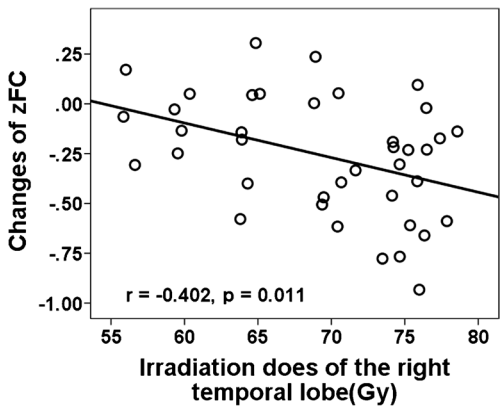

Fig. 6 Changes of the right insular FC correlated with the maximum irradiation dose in the right temporal lobe

Compared to the baseline, NPC patients had significantly reduced FC in the left ACC within the DMN, in the right insular within the SN and between bilateral ECN 3 months post-RT. It is not surprising that the ACC and insular showed aberrant FC, given that the ACC is a part of the limbic system and the insular is part of the paralimbic system, both regions which are sensitive to irradiation (Karunamuni et al. 2016; Makale et al. 2017). Previous studies also revealed that the limbic and temporal are more vulnerable to irradiation. For example, Karuna et al. (Karunamuni et al. 2016) found that dose-dependent cortical atrophy was particularly pronounced in the limbic and temporal lobes. Additionally, attenuated FC within the DMN and SN, and FC between the bilateral ECN, also agreed with previous cognitive studies, which indicated high-order cognition impaired, especially for memory, attention, and executive function, which was shown to be highly related to the DMN, ECN and SN in previous studies (Sestieri et al. 2011; Menon and Uddin 2010; Seeley et al. 2007). The present longitudinal study also agreed with the only extant cross sectional literature about RT-related FC in NPC: Ma et al. (2016) also revealed that the ACC, AI, and dorsal lateral prefrontal cortex (part of the ECN) had aberrant FC in NPC patients with RT when compared with demographically matched untreated NPC patients. However, they also found other network abnormalities. The reason for this discrepancy is unclear and could be due to differences such as post irradiation time (3 vs. 18 months) and analytical methods (ICA vs. MVPA classification) (Ma et al. 2016). More importantly, it might also due to the fact that cross sectional studies are influenced by between-subject variance and possible cohort effects (Schaie 2005) and are unable to detect the intra-individual alternation; thus, cross sectional comparison is insufficient to conclude the effects of RT effects on FC.

Interestingly, we found irradiation dose-dependent disruption of FC in the right insular, which indicates that FC impairment in the right insular has a cumulative effect, implying that reduced irradiation dose is important for this vulnerable region. Previous studies with diverse MRI models consistently revealed dose-dependent effects of irradiation related brain alternations (Karunamuni et al. 2016; Seibert et al. 2017; Wang et al. 2009). For instance, Karunamuni et al. (2016) found the dose-dependent cortical atrophy in high-grade glioma patients after partial brain radiation; moreover, they revealed that cortical atrophy was particularly pronounced in the limbic and temporal lobes, which echo the insular dose-dependent FC abnormalities revealed in the current study. Furthermore, Seibert et al. (2017) indicated that the hippocampus demonstrates radiation dose-dependent atrophy 1 year after treatment for patients who underwent fractionated, partial

brain RT for primary brain tumors when compared to the baseline. Lastly, Wang et al. (2009) found that a higher radiation dose (30 Gy) induced earlier and more severe histologic changes than a lower radiation dose (25 Gy), and these differences were reflected by the magnitude of changes in axial and radial diffusivity. Taken together, our findings add the dose-dependent functional network impairment to these extant literatures.

The functional network impairment observed in the current study may also due to the neurotoxicity of chemotherapy, given that most participants underwent concurrent chemotherapy, and chemotherapy itself had been related to both structural and functional brain disruption in previous studies (Dumas et al. 2013; McDonald and Saykin 2013; Iyer et al. 2015). However, the present results are more likely due to irradiation effects and not the chemotherapy, given that we did not find any chemotherapy related inter- or intra-network FC abnormalities in the subset of present participants who underwent BOLD-fMRI examination after chemotherapy but before the initial of RT. However, this negative finding may also be due to the relatively small sample size (n = 16) and short-term follow-up time (soon after chemotherapy). Thus, future studies should enroll RT only group to exclusively exclude the effects of chemotherapy.

We also found that general cognitive function declined post-RT, which is in line with previous studies that indicated RT-related cognition impairment (Greene-Schloesser and Robbins 2012; Makale et al. 2017). However, we did not find any relationship between network-level FC and cognition, which may due to the insensitivity of the MoCA measurement. The MoCA is a brief cognitive screening tool (Nasreddine et al. 2005), which is not very sensitive to certain domains, such as executive functions, verbal and visual memory, and attention, that impaired by irradiation revealed by previous studies (Greene-Schloesser and Robbins 2012; Zhang et al. 2015). Thus, a more sophisticated cognitive evaluation should be performed in future studies.

We acknowledge some limitations of the present study. First, we did not have NPC- and treatment-negative groups for comparison. A previous study had indicated that a non-central nervous system tumor alone was sufficient to induce brain dysfunction (Yang et al. 2014), we cannot exclude such an effect in present study. Second, as mentioned above, the MoCA is a brief cognitive screening tool not very sensitive to certain domains, such as executive functions, verbal and visual memory, and attention, impaired by irradiation revealed by previous studies (Greene-Schloesser and Robbins 2012; Zhang et al. 2015). Thus, a more sophisticated cognitive evaluation should be performed in future studies. Third, almost all participants enrolled in present study had concurrent chemotherapy and RT, and although we did not find any chemotherapy-related FC changes in the sub-cohort, the effects of chemotherapy or the synergy of chemotherapy and RT may exist. Therefore, future studies should enroll chemotherapy and RT only groups to elucidate such effects.

Conclusions

Combining the analysis of intra- and inter- network FC provided new insights into the radiation-induced functional impairments in NPC patients early post-RT. Reduced within and between network FC may serve as potential biomarkers of the RT-induced brain functional impairments and provide valuable targets for further functional recovery treatment. Furthermore, the dose-dependent alternation in the right insular within the SN implied that a reduced irradiation dose is important for this vulnerable region.

Acknowledgements We thank LetPub (http://www.letpub.com) for its linguistic assistance during the preparation of this manuscript.

Funding This work was funded by grants from the Natural Scientific Foundation of China (grant numbers: 81401399, 81560283, and 81201084), Natural Scientific Foundation of Jiangxi Province, China (grant number: 20151BAB205049), Fundamental Research Funds for the Central Universities (Grant number: 15ykpy35), and Medical Scientific Research Foundation of Guangdong Province (Grant number: B2014162).

Compliance with ethical standards

Conflict of interest The authors declare that they have no conflict of interest.

Ethical approval All procedures performed in studies involving human participants were in accordance with the ethical standards of the institutional and/or national research committee and with the 1964 Helsinki declaration and its later amendments or comparable ethical standards.

Informed consent Informed consent was obtained from all individual participants included in the study.

References

Beckmann, C. F., DeLuca, M., Devlin, J. T., & Smith, S. M. (2005). Investigations into resting-state connectivity using independent component analysis. *Philosophical Transactions of the Royal Society of London. Series B, Biological Sciences, 360*(1457), 1001–1013. https://doi.org/10.1098/rstb.2005.1634.

Biswal, B., Yetkin, F. Z., Haughton, V. M., & Hyde, J. S. (1995). Functional connectivity in the motor cortex of resting human brain using echo-planar MRI. *Magnetic Resonance in Medicine, 34*(4), 537–541.

Bressler, S. L., & Menon, V. (2010). Large-scale brain networks in cognition: emerging methods and principles. *Trends in Cognitive Sciences, 14*(6), 277–290. https://doi.org/10.1016/j.tics.2010.04.004.

Calhoun, V. D., Adali, T., Pearlson, G. D., & Pekar, J. J. (2001). A method for making group inferences from functional MRI data using independent component analysis. *Human Brain Mapping, 14*(3), 140–151.

Calhoun, V. D., Liu, J., & Adali, T. (2009). A review of group ICA for fMRI data and ICA for joint inference of imaging, genetic, and ERP data. *Neuroimage, 45*(1 Suppl), 163–172. https://doi.org/10.1016/j.neuroimage.2008.10.057.

Damoiseaux, J. S., Rombouts, S. A., Barkhof, F., Scheltens, P., Stam, C. J., Smith, S. M., et al. (2006). Consistent resting-state networks across healthy subjects. *Proceedings of the National Academy of Sciences of the United States of America, 103*(37), 13848–13853. https://doi.org/10.1073/pnas.0601417103.

Dumas, J. A., Makarewicz, J., Schaubhut, G. J., Devins, R., Albert, K., Dittus, K., et al. (2013). Chemotherapy altered brain functional connectivity in women with breast cancer: a pilot study. *Brain Imaging and Behavior, 7*(4), 524–532. https://doi.org/10.1007/s11682-013-9244-1.

Ewers, M., Sperling, R. A., Klunk, W. E., Weiner, M. W., & Hampel, H. (2011). Neuroimaging markers for the prediction and early diagnosis of Alzheimer's disease dementia. *Trends in Neurosciences, 34*(8), 430–442. https://doi.org/10.1016/j.tins.2011.05.005.

Fox, M. D., Snyder, A. Z., Vincent, J. L., Corbetta, M., Van Essen, D. C., & Raichle, M. E. (2005). The human brain is intrinsically organized into dynamic, anticorrelated functional networks. *Proceedings of the National Academy of Sciences of the United States of America, 102*(27), 9673–9678. https://doi.org/10.1073/pnas.0504136102.

Greene-Schloesser, D., & Robbins, M. E. (2012). Radiation-induced cognitive impairment–from bench to bedside. *Neuro-Oncology, 14 Suppl, 4*, 37–44. https://doi.org/10.1093/neuonc/nos196.

Greicius, M. D., & Kimmel, D. L. (2012). Neuroimaging insights into network-based neurodegeneration. *Current Opinion in Neurology, 25*(6), 727–734. https://doi.org/10.1097/WCO.0b013e32835a26b3.

Gusnard, D. A., Raichle, M. E., & Raichle, M. E. (2001). Searching for a baseline: functional imaging and the resting human brain. *Nature Reviews Neuroscience, 2*(10), 685–694. https://doi.org/10.1038/35094500.

Hsiao, K. Y., Yeh, S. A., Chang, C. C., Tsai, P. C., Wu, J. M., & Gau, J. S. (2010). Cognitive function before and after intensity-modulated radiation therapy in patients with nasopharyngeal carcinoma: a prospective study. *International Journal of Radiation Oncology, Biology, Physics, 77*(3), 722–726. https://doi.org/10.1016/j.ijrobp.2009.06.080.

Hyvarinen, A. (1999). Fast and robust fixed-point algorithms for independent component analysis. *IEEE Transactions on Neural Networks, 10*(3), 626–634. https://doi.org/10.1109/72.761722.

Iyer, N. S., Balsamo, L. M., Bracken, M. B., & Kadan-Lottick, N. S. (2015). Chemotherapy-only treatment effects on long-term neurocognitive functioning in childhood ALL survivors: a review and meta-analysis. *Blood, 126*(3), 346–353. https://doi.org/10.1182/blood-2015-02-627414.

Jafri, M. J., Pearlson, G. D., Stevens, M., & Calhoun, V. D. (2008). A method for functional network connectivity among spatially independent resting-state components in schizophrenia. *Neuroimage, 39*(4), 1666–1681. https://doi.org/10.1016/j.neuroimage.2007.11.001.

Karunamuni, R., Bartsch, H., White, N. S., Moiseenko, V., Carmona, R., Marshall, D. C., et al. (2016). Dose-dependent cortical thinning after partial brain irradiation in high-grade glioma. *International Journal of Radiation Oncology, Biology, Physics, 94*(2), 297–304. https://doi.org/10.1016/j.ijrobp.2015.10.026.

Li, Y. O., Adali, T., & Calhoun, V. D. (2007). Estimating the number of independent components for functional magnetic resonance imaging data. *Human Brain Mapping, 28*(11), 1251–1266. https://doi.org/10.1002/hbm.20359.

Lin, H., Huang, S., Deng, X., Zhu, J., & Chen, L. (2014). Comparison of 3D anatomical dose verification and 2D phantom dose verification of IMRT/VMAT treatments for nasopharyngeal carcinoma. *Radiation Oncology, 9*, 71. https://doi.org/10.1186/1748-717X-9-71.

Lv, X. F., Qiu, Y. W., Tian, J. Z., Xie, C. M., Han, L. J., Su, H. H., et al. (2013a). Abnormal regional homogeneity of resting-state brain activity in patients with HBV-related cirrhosis without overt hepatic encephalopathy. *Liver International, 33*(3), 375–383. https://doi.org/10.1111/liv.12096.

Lv, X. F., Ye, M., Han, L. J., Zhang, X. L., Cai, P. Q., Jiang, G. H., et al. (2013b). Abnormal baseline brain activity in patients with HBV-related cirrhosis without overt hepatic encephalopathy revealed by resting-state functional MRI. *Metabolic Brain Disease, 28*(3), 485–492. https://doi.org/10.1007/s11011-013-9420-4.

Lv, X. F., Wu, H. W., Tian, L., Han, L. J., Li, J., Qiu, Y. W., et al. (2016). Aberrant resting-state functional connectivity density in patients with hepatitis B virus-related cirrhosis. *BioMed Research International, 2016*, 4168512, https://doi.org/10.1155/2016/4168512.

Ma, Q., Wu, D., Zeng, L.-L., Shen, H., Hu, D., & Qiu, S. (2016). Radiation-induced functional connectivity alterations in nasopharyngeal carcinoma patients with radiotherapy. *Medicine, 95*(29), e4275. https://doi.org/10.1097/md.0000000000004275.

Ma, X., Qiu, Y., Tian, J., Wang, J., Li, S., Zhan, W., et al. (2015). Aberrant default-mode functional and structural connectivity in heroin-dependent individuals. *PLoS One, 10*(4), e0120861. https://doi.org/10.1371/journal.pone.0120861.

Makale, M. T., McDonald, C. R., Hattangadi-Gluth, J. A., & Kesari, S. (2017). Mechanisms of radiotherapy-associated cognitive disability in patients with brain tumours. *Nature Reviews Neurology, 13*(1), 52–64. https://doi.org/10.1038/nrneurol.2016.185.

McDonald, B. C., & Saykin, A. J. (2013). Alterations in brain structure related to breast cancer and its treatment: chemotherapy and other considerations. *Brain Imaging and Behavior, 7*(4), 374–387. https://doi.org/10.1007/s11682-013-9256-x.

Menon, V. (2011). Large-scale brain networks and psychopathology: a unifying triple network model. *Trends in Cognitive Sciences, 15*(10), 483–506. https://doi.org/10.1016/j.tics.2011.08.003.

Menon, V., & Uddin, L. Q. (2010). Saliency, switching, attention and control: a network model of insula function. *Brain Structure and Function, 214*(5–6), 655–667. https://doi.org/10.1007/s00429-010-0262-0.

Nasreddine, Z. S., Phillips, N. A., Bedirian, V., Charbonneau, S., Whitehead, V., Collin, I., et al. (2005). The Montreal cognitive assessment, MoCA: a brief screening tool for mild cognitive impairment. *Journal of the American Geriatrics Society, 53*(4), 695–699. https://doi.org/10.1111/j.1532-5415.2005.53221.x.

Pospisil, P., Kazda, T., Hynkova, L., Bulik, M., Dobiaskova, M., Burkon, P., et al. (2017). Post-WBRT cognitive impairment and hippocampal neuronal depletion measured by in vivo metabolic MR spectroscopy: results of prospective investigational study. *Radiotherapy and Oncology, 122*(3), 373–379. https://doi.org/10.1016/j.radonc.2016.12.013.

Prust, M. J., Jafari-Khouzani, K., Kalpathy-Cramer, J., Polaskova, P., Batchelor, T. T., Gerstner, E. R., et al. (2015). Standard chemoradiation for glioblastoma results in progressive brain volume loss. *Neurology, 85*(8), 683–691. https://doi.org/10.1212/WNL.0000000000001861.

Qiu, Y. W., Han, L. J., Lv, X. F., Jiang, G. H., Tian, J. Z., Zhuo, F. Z., et al. (2011). Regional homogeneity changes in heroin-dependent individuals: resting-state functional MR imaging study. *Radiology, 261*(2), 551–559. https://doi.org/10.1148/radiol.11102466.

Qiu, Y. W., Jiang, G. H., Ma, X. F., Su, H. H., Lv, X. F., & Zhuo, F. Z. (2016). Aberrant interhemispheric functional and structural connectivity in heroin-dependent individuals. *Addiction Biology*. https://doi.org/10.1111/adb.12387.

Qiu, Y. W., Lv, X. F., Jiang, G. H., Su, H. H., Ma, X. F., Tian, J. Z., et al. (2017a). Larger corpus callosum and reduced orbitofrontal cortex homotopic connectivity in codeine cough syrup-dependent

male adolescents and young adults. *European Radiology, 27*(3), 1161–1168. https://doi.org/10.1007/s00330-016-4465-5.

Qiu, Y. W., Su, H. H., Lv, X. F., Ma, X. F., Jiang, G. H., & Tian, J. Z. (2017b). Intrinsic brain network abnormalities in codeine-containing cough syrup-dependent male individuals revealed in resting-state fMRI. *Journal of Magnetic Resonance Imaging, 45*(1), 177–186. https://doi.org/10.1002/jmri.25352.

Raichle, M. E., MacLeod, A. M., Snyder, A. Z., Powers, W. J., Gusnard, D. A., & Shulman, G. L. (2001). A default mode of brain function. *Proceedings of the National Academy of Sciences of the United States of America, 98*(2), 676–682. https://doi.org/10.1073/pnas.98.2.676.

Schaie, K. W. (2005). What can we learn from longitudinal studies of adult development? *Research in Human Development, 2*(3), 133–158. https://doi.org/10.1207/s15427617rhd0203_4.

Seeley, W. W., Menon, V., Schatzberg, A. F., Keller, J., Glover, G. H., Kenna, H., et al. (2007). Dissociable intrinsic connectivity networks for salience processing and executive control. *The Journal of Neuroscience, 27*(9), 2349–2356. https://doi.org/10.1523/JNEUROSCI.5587-06.2007.

Seibert, T. M., Karunamuni, R., Bartsch, H., Kaifi, S., Krishnan, A. P., Dalia, Y., et al. (2017). Radiation dose-dependent hippocampal atrophy detected with longitudinal volumetric magnetic resonance imaging. *International Journal of Radiation Oncology, Biology, Physics, 97*(2), 263–269. https://doi.org/10.1016/j.ijrobp.2016.10.035.

Sestieri, C., Corbetta, M., Romani, G. L., & Shulman, G. L. (2011). Episodic memory retrieval, parietal cortex, and the default mode network: functional and topographic analyses. *The Journal of Neuroscience, 31*(12), 4407–4420. https://doi.org/10.1523/JNEUROSCI.3335-10.2011.

Shehzad, Z., Kelly, A. M., Reiss, P. T., Gee, D. G., Gotimer, K., Uddin, L. Q., et al. (2009). The resting brain: unconstrained yet reliable. *Cerebral Cortex, 19*(10), 2209–2229. https://doi.org/10.1093/cercor/bhn256.

Shirer, W. R., Ryali, S., Rykhlevskaia, E., Menon, V., & Greicius, M. D. (2012). Decoding subject-driven cognitive states with whole-brain connectivity patterns. *Cerebral Cortex, 22*(1), 158–165. https://doi.org/10.1093/cercor/bhr099.

Simo, M., Vaquero, L., Ripolles, P., Gurtubay-Antolin, A., Jove, J., Navarro, A., et al. (2016). Longitudinal brain changes associated with prophylactic cranial irradiation in lung cancer. *Journal of Thoracic Oncology, 11*(4), 475–486. https://doi.org/10.1016/j.jtho.2015.12.110.

Smith, S. M., Fox, P. T., Miller, K. L., Glahn, D. C., Fox, P. M., Mackay, C. E., et al. (2009). Correspondence of the brain's functional architecture during activation and rest. *Proceedings of the National Academy of Sciences of the United States of America, 106*(31), 13040–13045. https://doi.org/10.1073/pnas.0905267106.

Soussain, C., Ricard, D., Fike, J. R., Mazeron, J. J., Psimaras, D., & Delattre, J. Y. (2009). CNS complications of radiotherapy and chemotherapy. *Lancet, 374*(9701), 1639–1651. https://doi.org/10.1016/S0140-6736(09)61299-X.

Sridharan, D., Levitin, D. J., & Menon, V. (2008). A critical role for the right fronto-insular cortex in switching between central-executive and default-mode networks. *Proceedings of the National Academy of Sciences of the United States of America, 105*(34), 12569–12574. https://doi.org/10.1073/pnas.0800005105.

Storey, J. D. (2002). A direct approach to false discovery rates. *Journal of the Royal Statistical Society Series B-Statistical Methodology, 64*, 479–498. https://doi.org/10.1111/1467-9868.00346.

Sultanem, K., Shu, H. K., Xia, P., Akazawa, C., Quivey, J. M., Verhey, L. J., et al. (2000). Three-dimensional intensity-modulated radiotherapy in the treatment of nasopharyngeal carcinoma: the University of California-San Francisco experience. *International Journal of Radiation Oncology, Biology, Physics, 48*(3), 711–722.

Tang, Y., Luo, D., Rong, X., Shi, X., & Peng, Y. (2012). Psychological disorders, cognitive dysfunction and quality of life in nasopharyngeal carcinoma patients with radiation-induced brain injury. *PLoS One, 7*(6), e36529. https://doi.org/10.1371/journal.pone.0036529.

van de Ven, V. G., Formisano, E., Prvulovic, D., Roeder, C. H., & Linden, D. E. (2004). Functional connectivity as revealed by spatial independent component analysis of fMRI measurements during rest. *Human Brain Mapping, 22*(3), 165–178. https://doi.org/10.1002/hbm.20022.

Wang, S., Wu, E. X., Qiu, D., Leung, L. H., Lau, H. F., & Khong, P. L. (2009). Longitudinal diffusion tensor magnetic resonance imaging study of radiation-induced white matter damage in a rat model. *Cancer Research, 69*(3), 1190–1198. https://doi.org/10.1158/0008-5472.CAN-08-2661.

Wei, W. I., & Kwong, D. L. (2010). Current management strategy of nasopharyngeal carcinoma. *Clinical and Experimental Otorhinolaryngologica, 3*(1), 1–12. https://doi.org/10.3342/ceo.2010.3.1.1.

Wei, W. I., & Sham, J. S. (2005). Nasopharyngeal carcinoma. *Lancet, 365*(9476), 2041–2054. https://doi.org/10.1016/S0140-6736(05)66698-6.

Xu, C., Zhang, L. H., Chen, Y. P., Liu, X., Zhou, G. Q., Lin, A. H., et al. (2017). Chemoradiotherapy versus radiotherapy alone in stage II nasopharyngeal carcinoma: a systemic review and meta-analysis of 2138 patients. *Journal of Cancer, 8*(2), 287–297. https://doi.org/10.7150/jca.17317.

Yang, M., Kim, J., Kim, J. S., Kim, S. H., Kim, J. C., Kang, M. J., et al. (2014). Hippocampal dysfunctions in tumor-bearing mice. *Brain, Behavior, and Immunity, 36*, 147–155. https://doi.org/10.1016/j.bbi.2013.10.022.

Zhang, D., & Raichle, M. E. (2010). Disease and the brain's dark energy. *Nature Reviews Neurology, 6*(1), 15–28. https://doi.org/10.1038/nrneurol.2009.198.

Zhang, L. Y., Yang, H. Y., & Tian, Y. (2015). Radiation-induced cognitive impairment. *Therapeutic Targets for Neurological Diseases, 2*, e837. https://doi.org/10.14800/ttnd.837.